All-Optical Reconstruction of Crystal Band Structure

G. Vampa, T. J. Hammond, N. Thiré, B. E. Schmidt, F. Légaré, C. R. McDonald, T. Brabec, D. D. Klug, and P. B. Corkum

Phys. Rev. Lett. **115**, 193603 — Published 5 November 2015

DOI: 10.1103/PhysRevLett.115.193603

All optical reconstruction of a crystal's band structure

G. Vampa[1*], T. J. Hammond[1], N. Thiré[2], B. E. Schmidt[2], F. Légaré[2], C. R. McDonald[1], T. Brabec[1], D. D. Klug[3] and P. B. Corkum[1,3]

[1]*Department of Physics, University of Ottawa, Ottawa, ON K1N 6N5, Canada.*

[2]*INRS-EMT, 1650 Boulevard Lionel-Boulet, CP 1020, Varennes, Québec J3X 1S2, Canada.*

[3]*National Research Council of Canada, Ottawa, ON K1A 0R6, Canada.*

PACS: 42.65.Ky, 71.90.+q, 72.20.Ht, 42.50.Hz

*Correspondence to: gvamp015@uottawa.ca or paul.corkum@nrc.ca.

The band structure of matter determines its properties. In solids, it is typically mapped with angle-resolved photoemission spectroscopy, in which the momentum and the energy of incoherent electrons are independently measured. Sometimes, however, photoelectrons are difficult or impossible to detect. Here we demonstrate an all-optical technique to reconstruct momentum-dependent bandgaps by exploiting the coherent motion of electron-hole pairs driven by intense mid-infrared femtosecond laser pulses. Applying the method to experimental data for a semiconductor ZnO crystal we identify the split-off valence band as making the greatest contribution to tunnelling to the conduction band. Our new band structure measurement technique is intrinsically bulk sensitive, does not require vacuum, and has high temporal resolution, making it suitable to study reactions at ambient conditions, matter under extreme pressures and ultrafast transient modifications to band structures.

As explained by Einstein in 1905 [1], when a photon of sufficient energy $h\nu$ impinges on a material, it liberates an electron with kinetic energy $K=h\nu - W - E$, where W is the work function of the material and E is the binding energy of the electron in it. The process is depicted in the left side of Fig. 1. If the kinetic energy and the vector momentum of the electron are measured, the momentum-dependent binding energy $\varepsilon(k)$, or the "structure" of the occupied bands, can be obtained. This is the working principle of Angle-Resolved PhotoEmission Spectroscopy (ARPES) [2], the key tool to understand novel systems, such as high-temperature superconductors [3,4] and other strongly correlated materials like graphene [5-7] and topological insulators [8,9]. Conversely, in "inverse photoemission" [10], an electron can be externally injected into higher-lying unoccupied bands and the photon emitted upon its decay to lower-lying states is measured.

We discuss a coherent analogue to inverse photoemission, in which we measure photons emitted upon recombination of electron-hole pairs that are internally created and accelerated by a strong laser field. By linking photon energy to momentum of the pair at recombination, we map the momentum-dependent bandgap between the bands occupied by the electron and the hole.

The possibility of using the non-destructive interaction with intense laser fields of photon energies ~ 1 eV has gained relevance only recently [11-13]. A laser field with photon energy much smaller than the minimum bandgap of a semiconductor crystal generates high odd order harmonics of its fundamental frequency when focused to reach an electric field as strong as a few V/Å [11]. Under such a strong field an electron first tunnels from the top of the valence to the

bottom of the conduction band (circled “1” in Fig. 1). The electron and the hole are then accelerated to high crystal momentum (circled “2” in Fig. 1), travelling a significant portion of the Brillouin Zone along the laser polarization and, during this process, storing information about the underlying band. In space, they are accelerated in opposite directions with a velocity determined by the band in which they move. Information about the bands is imprinted on a short wavelength photon when the field reverses direction and the electron and the hole are driven back towards each other. Upon re-encounter, they can recombine (with a vertical transition) at a crystal momentum that is determined by the time of creation of the pair, emitting a harmonic photon in the process with energy equal to the bandgap at the momentum of re-encounter [14] (circled “3” in Fig. 1). Two of these trajectories are identified by the wiggled solid arrows during step “2” in Fig. 1. Knowledge of the trajectory links photon energy to momentum of the recolliding electron-hole pair, in a similar fashion that photoelectron energy is linked to its momentum in ARPES. However, high harmonic generation from solids does not require vacuum. A recent experiment proved that recollision and recombination of the electron-hole pair dominates over other competing mechanisms for excitation with mid-infrared laser pulses [15]. For longer (THz) [16] and shorter (near-infrared) pulses [17], the recollision contribution to the high harmonics is suppressed. Therefore, in the following we focus our attention to harmonics obtained from recollision.

Information about the trajectories, and therewith about the band structure, is obtained by perturbing the high harmonic generation process with a weak second harmonic field [18,15], thereby producing even harmonics. Their strength modulates as the second harmonic is delayed relative to the fundamental. A simulated spectrogram is shown in Fig. 2a for a model hexagonal

crystal interacting with a fundamental mid-infrared laser pulse and its second harmonic (at an intensity of 10^{-5} of the fundamental). The fundamental field has a peak strength of 0.28 V/Å and a central wavelength of 3.66 μm; both fields are linearly polarized along the $\Gamma - M$ direction of the Brillouin Zone. Details about the simulation are reported in the Online Supplementary Material (OSM) [19]. The phase of the modulation Φ_{osc}, plotted as red dots with error bars in Fig. 2b, differs between harmonic orders. It is this quantity that uniquely tags the trajectories and identifies the band structure of the material. A realistic experimental uncertainty on Φ_{osc} is ~ 25 mrad, and is artificially added to simulate noise in an experiment. The bandgap between the valence and conduction bands is plotted in Fig. 2c, red line, up to the edge of the Brillouin Zone. Its analytical form is reported in the caption of Fig. 2. This is the "target" band structure for a reconstruction procedure.

To understand the origin of the even harmonics and their intensity modulation it is useful to compare the high harmonic generation process to a balanced interferometer [18]: the odd harmonic structure in the presence of the fundamental field arises from the interference of two equal but oppositely directed recollisions at subsequent half laser cycles – corresponding to two equal length arms of the interferometer. The second harmonic breaks this symmetry by lengthening one arm while shorting the other, therefore leading to imperfect interference and the appearance of the even harmonics – the interferometer is unbalanced. The optimum delay Φ_{osc} that leads to maximum even harmonic emission, corresponding to maximum symmetry breaking, differs between even harmonic orders because each trajectory is launched and is terminated at different times, and therefore experiences the second harmonic differently.

To reconstruct the target bandgap, we compare Φ_{osc} of the simulated experiment with those calculated for a set of trial bandgaps and find the ones that best reproduce the target (the procedure is detailed in the OSM). We use the χ^2 probability distribution to reject candidate band structures that badly fit the experimental phase: a trial is rejected if the probability of measuring $\chi^2 > \chi_{trial}^2$ is lower than the threshold $p = 0.1$. With a confidence level (1-p) of 90%, only four trial bands are plausible – their shape and the associated Φ^s_{osc} are plotted as grey lines in Figs. 2b-c. The retrieved band gaps are extremely accurate: at most they differ by 0.2 eV at M, a resolution comparable to time-resolved ARPES [4,6] (static experiments have higher resolution [3]). The accuracy is limited by the precision on Φ_{osc} and the number of measured harmonic orders (their effect on the reconstruction is analysed in the OSM), not by the spectral bandwidth of the laser pulse, a typical shortcoming of photoemission. In fact, shorter pulses (wider bandwidths) might even be beneficial to solid high harmonics because they can extend the harmonic cutoff (wider harmonic range), similarly to the atomic case [21]. The reconstruction assumes a known minimum band gap. It can be accurately measured with linear optical methods. In the OSM we show how the reconstruction is successful also for target and trial bandgaps with different functional forms. The momentum resolution (δk in Fig. 2c) can be interpreted as the difference between the maximum and minimum momentum corresponding to a given energy for the set of reconstructed bands. It amounts to ~ 1-5% of the Brillouin Zone, or to ~ 0.02-0.12 $Å^{-1}$.

In the simulated reconstruction presented so far, we need radiation stretching up to the maximum band energy to obtain the full relative band structure. In ZnO this requires a spectrum that terminates at ~ 10 eV. However, our spectrograph does not allow measurement beyond ~ 6 eV, or the 18^{th} harmonic. Therefore, we measure electrons and holes that explore only ~20% of the

112 Brillouin Zone. In the OSM (Fig. S3) we show that extrapolating the band structure to energies
113 higher than the measured harmonic range heavily depends on the functional form of the trials
114 and, in general, results in rapid loss of accuracy. With the limited experimental data presented in
115 Fig. 3a, we can identify which of the possible valence bands contribute to tunnelling. When
116 multiple occupied states contribute to high harmonic generation in atoms, a hole wavepacket is
117 launched and evolves on attosecond timescales [22]. Do similar dynamics exist in ZnO?

118 The experimental Φ_{osc} (black dots in Fig. 3b) agrees with the simulation for tunneling from the
119 split-off valence band to the first conduction band (green line); the other two curves associated to
120 tunneling from the heavy holes (gold) and light holes (red) bands are significantly steeper.
121 Therefore, hole dynamics don't seem to be initiated in ZnO. Here, the selected bands of ZnO are
122 obtained from *ab inito* calculation. Therefore, no reconstruction is performed.
123 Contrary to the situation of Figure 2, here we use an unmeasured offset phase to position the
124 experimental data. This phase is in principle measurable in more refined experiments, but is
125 strictly not required to completely reconstruct the band structure (see discussion in the OSM and
126 Figs. S4-6). The different slope of Φ_{osc} for the different valence bands is, to first order, related to
127 the effective mass: in narrow bands, adjacent harmonic orders map onto very different momenta,
128 and in turn to very different trajectories. Since the optimum phase is linked to the trajectory, Φ_{osc}
129 varies more strongly with harmonic order than in wider bands. The accuracy on Φ_{osc} is 50 mrad
130 and is mainly limited by intensity fluctuations on the high harmonic signal and delay jitter. The
131 bands are plotted in Fig. 3c, with the same color coding (blue for the conduction band).

132

133 The dominant contribution of the split-off valence band to tunnelling is expected: holes in this
134 band have a lower effective mass than the heavy and light holes valence bands. Is it possible to

reconstruct the heavier bands instead? It may be possible if the selected band is non degenerate with the split-off band (the separation is ~ 0.1 eV at Γ). For example, the infrared field could resonantly populate an intragap impurity level that lays one or two photon energies above the top of the desired valence band. From there, electrons will tunnel to the conduction band. The presence of the resonance greatly enhances tunneling over the off-resonant transitions from the split-off band. If the desired band is well separated (> 1 eV), one could also excite with a resonant ultraviolet pulse within a fraction of the infrared cycle [23].

Before concluding we will address three important issues. First, the electron and hole move in the bands dressed with the laser field. Does any laser field that is sufficiently intense to create the harmonics severely distort the bands we measure? As detailed in the OSM, the maximum calculated perturbation to the field-free states is only 2% of the bandgap. Furthermore, the simulations naturally include the effect of the field so that any distortion to Φ_{osc} is already accounted for in the reconstruction. Second, real materials have multiple bands. Does the presence of multiple bands alter the optimum phase originating from a two-band recombination? In this regard, recent calculations are encouraging. Model results show that two-band emission dominates over a reasonably extended intensity range [24,25]. This is possibly a result of the wide separation between bands. Coupling between multiple bands is expected to be negligible also for closely spaced bands of similar symmetry. When transition dipole moments become large, however, coupling of multiple bands can be significant [26]. Third, dynamical screening of the Coulomb interaction following strong-field excitation can lead to renormalization of the bandgap [13], and consequently to an offset of the absolute phase. In the OSM we show that for variations < 0.2 eV, the offset is almost identical for all harmonic orders,

158 and the reconstruction converges to the field-free band structure if the absolute phase is
159 neglected. Conversely, the absolute phase can be used to map the dynamical screening.

160

161 In summary, we have demonstrated an all-optical method for measuring band structures based on
162 high harmonic generation – a method complementary to ARPES. Specifically, we have shown
163 that the phase of the oscillation of even harmonics is sensitive to the momentum-dependent
164 bandgap. The technique that we have introduced will be useful where it is not possible to detect
165 photoelectrons, such as in the bulk of materials or in matter under extreme pressures [27,28] or
166 high magnetic fields. In addition, it may be possible to extend the approach to studying the
167 energetics of chemical reactions under ambient conditions (it does not require vacuum), such as
168 catalysis [29], oxidation of metals [30], and solution chemistry [31,32].

169 Due to the brief life of the recolliding electron-hole pair, all-optical band structure measurement
170 inherently has ultrafast temporal resolution [33], at no expense of energy resolution. It is now
171 possible to probe the fastest modifications to band structures, for example band renormalization
172 as population is transferred between the bands [13], the onset of screening [34] or of the effective
173 mass [35]. The initial states of photoinduced transitions in strongly correlated materials can
174 potentially be mapped, too [36,37].

175

176 The method can be extended to measure band structures in crystals that lack inversion symmetry,
177 for which even harmonics are produced by the fundamental field alone. For example, a second
178 harmonic beam non-collinear with the fundamental [38] can produce even harmonics that
179 spatially separate from those produced by the fundamental.

Finally, as in photoelectron spectroscopy, it seems possible to obtain information about individual bands by forcing the electron or the hole to propagate in a known band. For example a localized intragap impurity state for the hole or a free-electron band for an electron propagating in vacuum. The latter can be achieved by grazing incidence illumination with laser polarization orthogonal to the surface.

Acknowledgments: It is our pleasant duty to thank A. Laramée, from the Advanced Laser Light Source, for his technical assistance during the experiment. The authors also acknowledge valuable support from The US AFOSR and Canada's NRC, NSERC, FRQNT, and CFI-MSI (Major Science Initiatives).

References

1. A. Einstein, *Annalen der Physik* **17**, 132-148 (1905).
2. A. Damascelli, Z. Hussain and Z. X. Shen, *Reviews of modern physics* **75**, 473 (2003).
3. A. Lanzara, *et al*, *Nature* **412**, 510-514 (2001).
4. L. Perfetti, *et al., Phys. Rev. Lett.* **99**, 197001 (2007).
5. A. Bostwick, *et al*., *Nature Phys*. **3**, 36-40 (2007).
6. S. Ulstrup, *et al., Phys. Rev. Lett.* **112**, 257401 (2014).
7. S. Y. Zhou, *et al*., *Nature Mater*. **6**, 770-775 (2007).
8. Y. L. Chen, *et al*., *Science* **325**, 178-181 (2009).
9. X. Xia, *et al., Nature Phys*.**5**, 398-402 (2009).

10. V. Dose, *Surface Science Reports* **5**, 337-378 (1985).

11. S. Ghimire, *et al*., *Nature physics* **7**, 138-141 (2011).

12. A. Schiffrin, *et al., Nature* **493**, 70-74 (2013).

13. M. Schultze, *et al., Science* **346**, 1348-1352 (2014).

14. G. Vampa, *et al*., *Phys. Rev. Lett.* **113**, 073901 (2014).

15. G. Vampa, *et al., Nature* **522,** 462-464 (2015).

16. O. Schubert, *et al., Nature Photonics* **8**, 119-123 (2014).

17. T. T. Luu, *et al., Nature* **521**, 498-502 (2015).

18. N. Dudovich, *et al*., *Nature Physics* **2**, 781-786 (2006).

19. See Supplemental Material [url], which includes Ref. [20].

20. M. Lewenstein, P. Balcou, M. Y. Ivanov, A. L'Huillier and P. B. Corkum, *Phys. Rev. A* **49**, 2117 (1994).

21. B. E. Schmidt, *et al., J. Phys. B: At. Mol. Opt. Phys.* **45**, 074008 (2012).

22. E. Goulielmakis, *et al., Nature* **466**, 739-743 (2010).

23. J. Leeuwenburgh, *et al., Phys. Rev. Lett.* **111**, 123002 (2013).

24. M. Wu, S. Ghimire, D. A. Reis, K. J. Schafer and M. B. Gaarde, *Phys. Rev. A* **91**, 043839 (2015).

25. C. R. McDonald, G. Vampa, P. B. Corkum and T. Brabec, *Phys. Rev. A.* (to be published).

26. M. Hohenleutner, *et al., Nature* **523**, 572-575 (2015).

27. M. I. Eremets and I. A. Troyan, *Nature materials* **10**, 927-931 (2011).

28. J. Lv, Y. Wang, L. Zhu and Y. Ma, *Phys. Rev. Lett.* **106**, 015503 (2011).

29. F. Tao, *et al., Science* **322**, 932 (2008).

30. G. Ketteler, *et al., J. Am. Chem. Soc.* **127**, 18269-18273 (2005).

31. H. Bluhm, *J. Electron Spectrosc. Relat. Phenom.* **177**, 71-84 (2010).

32. J. Ghosal, *et al., Science* **307**, 563-566 (2005).

33. S. Baker, *et al.*, *Science* **312**, 424-427 (2006).

34. R. Huber, *et al., Nature* **414**, 286-289 (2001).

35. R. Chang, *et al., Phys. Rev. Lett.* **112**, 170404 (2014).

36. L. Perfetti, *et al.*, *Phys. Rev. Lett.* **97**, 067402 (2006).

37. M. Rini, *et al., Optics letters* **30**, 558-560 (2005).

38. K. T. Kim, *et al., Nature Physics* **9**, 159-163 (2014).

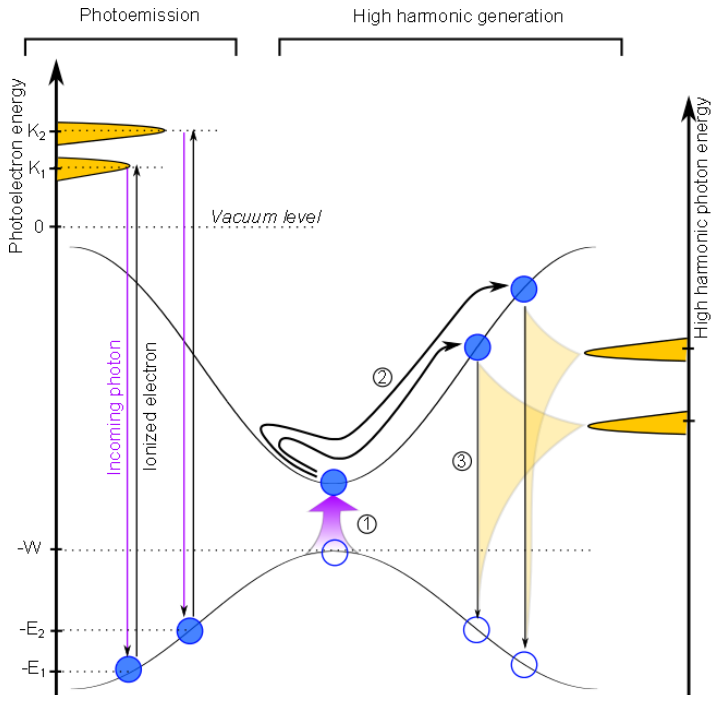

FIG 1 Comparison between photoemission and high harmonic generation. In photoemission experiments, an incoming photon (purple arrow) causes emission of an electron (black vertical arrow) with kinetic energy (K_1 and K_2) proportional to the initial binding energy (E_1 and E_2). In high harmonic generation, an electron first tunnels (marked by circled "1") to the conduction band. The electron-hole pair is then accelerated (circled "2") and recombines (circled "3")

emitting a harmonic photon in the process. Electrons and holes are denoted by filled and empty blue circles respectively. Two trajectories are identified by the wiggled solid black arrows, corresponding to different times of creation and recollision of the electron-hole pair.

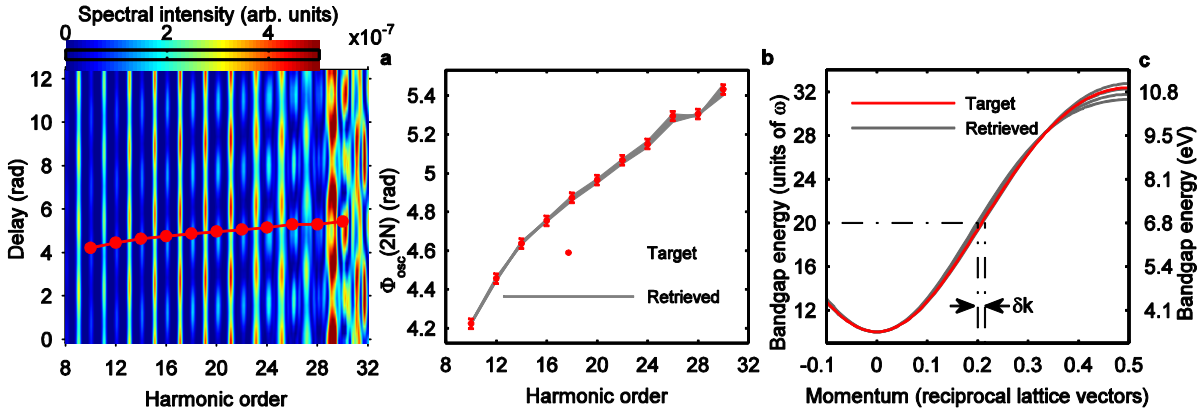

FIG 2 Reconstruction of the bands. (a) High harmonic spectrum obtained from the target band structure as a function of delay between fundamental and second harmonic fields. The red line with dots is the optimum phase Φ_{osc}. (b) Target Φ_{osc} (red dots with error bars) compared to those associated with the retrieved band structures (grey lines). (c) Target (red line) and retrieved (grey lines) momentum-dependent bandgaps. The Brillouin Zone extends up to half of the reciprocal lattice vector. The target bandgap is $\varepsilon(k)=\varepsilon_g + 0.139\,[1 - \cos(ka)] + 0.011\,[1 - \cos(2ka)]$, and approximates that of a ZnO crystal as obtained from *ab initio* calculations. The crystal and laser parameters are defined in Table S2 of the OSM.

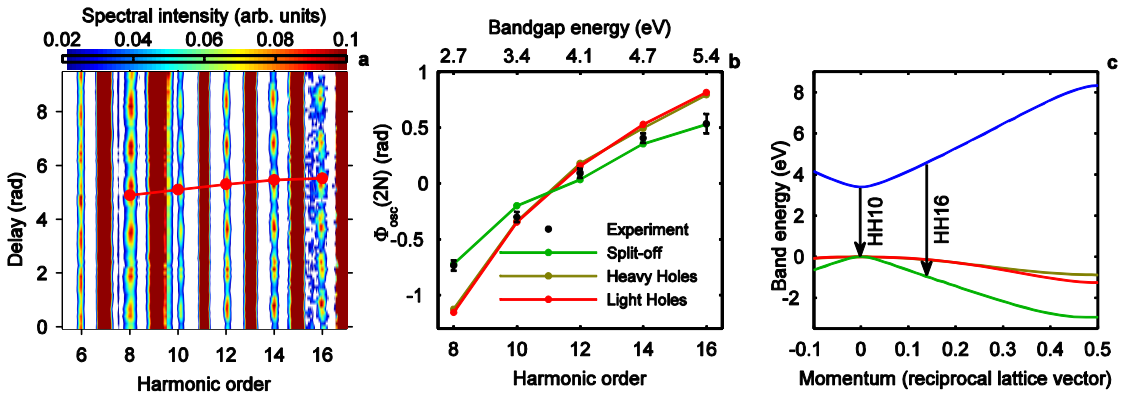

FIG 3 Experimental contribution of the split-off band. (a) Experimental spectrogram obtained from a ZnO crystal. Experimental parameters are the same as in Fig. 2. Each harmonic order is independently normalized to facilitate comparison between orders. The odd harmonics saturate the spectrometer. The red line is the experimental Φ_{osc}. (b) The optimum phase extracted from the experiment (black dots with error bars), simulated for tunneling from the split-off valence band (green line), the heavy-holes band (gold line) and the light holes band (red line). Contrary to Fig. 2, here we use an unmeasured offset phase to position the experimental data. This phase is in principle measurable in a more refined experiment. (c) Band structure for the same bands of part (b) with the same color coding. The blue band is the first conduction band. They are obtained from *ab initio* calculations. The arrows mark the recombination between electrons and holes in the split-off band for the 10^{th} and 16^{th} harmonic orders. The measured harmonic spectrum extends up to ~25% of the Brillouin Zone.